Surge of Hispar Glacier, Pakistan, between 2013 and 2017 detected from remote sensing observations

Rashid, Irfan; Abdullah, Tariq; Glasser, Neil; Naz, Heena; Romshoo, Shakil Ahmad

Published in:
Geomorphology

DOI:
10.1016/j.geomorph.2017.12.018

Publication date:
2018

Citation for published version (APA):
Rashid, I., Abdullah, T., Glasser, N., Naz, H., & Romshoo, S. A. (2018). Surge of Hispar Glacier, Pakistan, between 2013 and 2017 detected from remote sensing observations. *Geomorphology*, *303*, 410-416. https://doi.org/10.1016/j.geomorph.2017.12.018

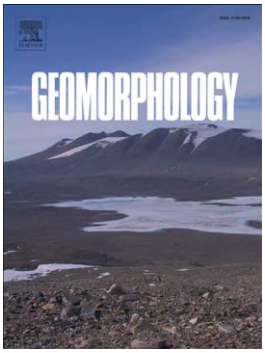

Surge of Hispar Glacier, Pakistan, between 2013 and 2017 detected from remote sensing observations

Irfan Rashid, Tariq Abdullah, Neil F. Glasser, Heena Naz, Shakil Ahmad Romshoo

PII: S0169-555X(17)30527-5
DOI: doi:10.1016/j.geomorph.2017.12.018
Reference: GEOMOR 6259

To appear in: *Geomorphology*

Received date: 22 April 2017
Revised date: 8 December 2017
Accepted date: 11 December 2017

Please cite this article as: Rashid, Irfan, Abdullah, Tariq, Glasser, Neil F., Naz, Heena, Romshoo, Shakil Ahmad, Surge of Hispar Glacier, Pakistan, between 2013 and 2017 detected from remote sensing observations, *Geomorphology* (2017), doi:10.1016/j.geomorph.2017.12.018

This manuscript is submitted for publication in *Geomorphology*

Title:

Surge of Hispar Glacier, Pakistan, between 2013 and 2017 detected from remote sensing observations

Author List:

Irfan Rashid[1*], Tariq Abdullah[1], Neil F. Glasser[2], Heena Naz[1], Shakil Ahmad Romshoo[1]

Corresponding Author Email: irfangis@gmail.com
irfangis@kashmiruniversity.ac.in

Author Affiliations:

[1]Department of Earth Sciences, University of Kashmir, Hazratbal Srinagar, Jammu and Kashmir, 190006, India

[2]Centre for Glaciology, Department of Geography and Earth Sciences, Aberystwyth University, Aberystwyth, Wales, SY23 3DB, UK

Running Head:

Surge of Hispar Glacier from remote sensing observations

Abstract

This study analyses the behaviour of an actively surging glacier, Hispar, in Pakistan using remote sensing methods. We used 15m panchromatic band of Landsat 8 OLI from 2013 - 2017 to assess the changes in glacier velocity, glacier geomorphology and supraglacial water bodies. For the velocity estimation, correlation image analysis (CIAS) was used, which is based on normalized cross-correlation (NCC) of satellite data. On-screen digitization was employed to quantify changes in the glacier geomorphology and dynamics of supraglacial water bodies on the glacier. Our velocity estimates indicate that the upper part of the glacier is presently undergoing an active surge which not only affects the debris distribution but also impacts the development of supraglacial water bodies. Velocities in the actively surging part of the main glacier trunk and its three tributaries reach up to ~900 m yr^{-1}. The surge of Hispar also impacts the distribution of supraglacial debris causing folding of the medial moraines features present on the glacier surface. Changes in the number and size of supraglacial lakes and ponds was also observed during the observation period from 2013-2017.

Keywords: Glacier surge; Karakoram; Supraglacial water bodies; Glacier velocity

1. Introduction

Glacier surges have been reported from many areas of the world including the Canadian and Russian High Arctic, Svalbard, Iceland, Greenland, Alaska and parts of the Himalaya (Sevestre and Benn, 2015). These surge-type glaciers go through an active phase and a quiescent phase. While the active phase is characterised by recurring non-steady flow that can last for a few months to years, the quiescent phase lasts longer, typically tens to few hundreds of years (Meier and Post, 1969). Karakoram glacier surges are poorly understood (Hewitt, 2005). The glacier velocities of surge-type glaciers in Karakoram during active phase increase by up to 200% than during the quiescent phase (Hewitt, 1969). Peak velocities of around 2 km yr^{-1}during summer months have been observed (Quincey et al., 2015). Majority of the surge type glacier have been reported to vary between 12 and 25 km in length (Hewitt, 1969) and are often fed by tributary glaciers (Hewitt, 2007). There is a positive correlation between surge-type glaciers and glacier length, area, perimeter, average width, debris cover and orientation (Barrand and Murray, 2006). Insignificant changes in debris cover, indicative of stable mass budget of glaciers in Hunza river basin, has been recently reported (Herreid et al. 2015; Bolch et al. 2017). The season of Karakoram glacier surge initiation varies. Some surges develop extremely quickly (Kick, 1958; Gardner and Hewitt, 1990) while others develop gradually over several years (Quincey et al., 2011). These surges can result in huge advance of the glacier snout (km-scale), over a short time span (weeks to months). It has been suggested that Karakoram glacier surges may be triggered by change in thermal conditions (Hewitt, 2007) that coincide with warming driven by long-duration precipitation patterns (Quincey et al., 2011), although other studies advocated changes in hydrological conditions as a possible trigger mechanism for glacier

surges in the region (Copland et al., 2011; Mayer et al., 2011). However, it is pertinent to mention that the glacial hydrological regimes are controlled by the thermal regimes.

Drawing on data from eight glaciers, Quincey et al. (2015) suggested that no single classical mechanism is able to comprehensively describe the flow-instability of surge-type glaciers in Karakoram. Their analysis did not find any evidence of seasonal control on the initiation of glacier surges in the region. They suggested that these surge events are triggered by a blend of hydrological and thermal processes.

Here we present new data concerning glacier velocity and changes in the surface character of a surge-type glacier in Pakistan, the Hispar Glacier. Hispar is a ~50 km long surge-type glacier (Copland et al 2011; Hewitt 2005), located in the Karakoram Mountains (Lat: 36.02-36.32 N; Lon: 75.02-75.55 E) in Gilgit Baltistan province of Pakistan (Figure 1). The mountains enclosing Hispar and its tributaries are characterized by very steep snow-covered cliffs rising to slope angles of 77^{o} which result in numerous snow avalanches feeding the glacier. The altitudinal extent of Hispar Glacier is 3088 to 7113 m amsl. Taking snow-line as an approximation of equilibrium line altitude (ELA), the ELA of the Hispar glacier lies at an elevation of 4956 m amsl. The Hispar River originates from the melt waters of the glacier. The glacier topography was first surveyed by Workman (1910) in 1908 who reported the presence of thick debris cover and crevasses across the ablation zone of the glacier. The snout of the glacier lies 2.42 km east of Hispar village at an altitude of 3088 m amsl. Hispar ascends with a gentle gradient in south easterly direction for 50 km to the highest point - Hispar pass (5335 m amsl), where it meets the upper extremity of the Biafo Glacier.

2. Data and Methods:

2.1. Data:

Landsat 8 OLI panchromatic band images with a spatial resolution of 15m, acquired between 2013 and 2017, were used for velocity estimation and glacial geomorphological mapping. Autumn images were chosen as they have the least snow and cloud cover in this region. The details of the datasets are given in Table 1.

2.2. Velocity:

Glacier surface velocity was estimated using a feature-tracking method based on automatic matching of satellite image pairs. A number of feature-tracking techniques have been applied in glaciological studies, including normalized cross-correlation (NCC), Fourier cross-correlation, least squares matching, phase correlation and orientation correlation (Kääb, 2005; Heid and Kääb, 2012). The present study used the correlation image analysis (CIAS) algorithm (Kääb and Vollmer, 1999) for glacier velocity estimation. This cross-correlation algorithm computes the displacement of prominent glacier surface features on two satellite images acquired at different points in time (Kääb and Vollmer, 2000) as:

$$\frac{\phi(i,k)=\sum_{j}\sum_{l} s\left[(i+j,k+l)-\left(\frac{T_{test}}{N_{test}}\right)\right]\times m\left[(j,l)-\left(\frac{T_{ref}}{N_{ref}}\right)\right]}{\sqrt{\left\{\sum_{j}\sum_{l} s^{2}\left[(i+j,k+l)-\left(\frac{T_{test}}{N_{test}}\right)\right]\times\sum_{j}\sum_{l} m^{2}\left[(j,l)-\left(\frac{T_{ref}}{N_{ref}}\right)\right]\right\}}} \quad (1)$$

The ϕ in the equation is the double cross-correlation function. The coordinates in the test and reference block are represented by (i, k) and (j, l) respectively. The spatial grey value function in the test block is represented by s and s, l, k is the corresponding grey value at location (i, k). Similarly m, j, l is the grey value at location (j, l) in the reference block represented by grey level function m. T is

the sum of grey values of the test or reference block, and N is the number of pixels of the test or reference block ($N_{ref} = N_{test}$).

Owing to its operational simplicity and robustness, CIAS is reliable for glacier velocity estimation (Heid and Kääb, 2012). The velocity measurements in NCC are carried out by systematically correlating a block of pixel values from reference image (so-called 'reference block') to the pixel values in the test block. Landsat 8 OLI satellite images from 2013 - 2017 were used in the present study. The panchromatic band of both the images with 15m spatial resolution and sufficient visual contrast were utilised to estimate horizontal velocities. The horizontal displacements were then estimated automatically in two steps. First, in the orthorectified satellite image of time 1, a block of pixels, whose ground coordinates are known, is chosen as reference block. Based on the reference block, corresponding image pixels, called test block, are searched in the image of time 2.

The differences in central pixel coordinates of the reference and test block directly give the horizontal displacement between the images under consideration. The accuracy of NCC method employed in CIAS is $\pm$1 pixel, which is 15m in our case (Kääb and Vollmer, 2000). For the calculation of velocity of the Hispar glacier the reference block size of 15 pixels and a search area size of 50 pixels at a grid of 100 m was used (Paul et al. 2017).

2.3. Glacial geomorphology:

Debris cover mapping on the glacier surface was carried out using on-screen digitization (OSD) at 1:25000 scale using the satellite images from 2013-2017. OSD with cognitive inputs from the analyst was employed due to its advantage over digital classification algorithms in delineation of different landscape features in a

topographically rugged terrain where clouds and shadows pose problems in interpreting image elements (Rashid et al. 2010; Rashid and Abdullah, 2016). We also delineated lateral and medial moraines of the Hispar Glacier so that the effects of the surge could be better understood.

2.4. Supraglacial water bodies:

Supraglacial water bodies were also delineated using OSD at 1:25000 scale on the satellite images from 2013-2017. Owing to the medium resolution of data, we could only delineate those water bodies as polygons which had an area of more than 0.5 hectare (Ha). The supraglacial water bodies with a surface area greater than 0.5 hectare (Ha) were classified as lakes while water bodies with an area less than 0.5 Ha were digitized as point features and classified as ponds. A change detection analysis was then carried out to assess the change in both area and number of ponds for the 5-year period of observation (September 2013 to September 2017).

3. Results:

3.1. Velocity Changes:

The trunk glacier can be divided into three different zones with differential velocity regimes (Figure 3). The zone 1 (Z1) between the snout and tributary T1 had the lowest velocities during the assessment period. The average velocity in this zone is ~30 m yr^{-1}. The zone 2 (Z2) that extends from just above the convergence of T1 with the main trunk to point B just below the ice fall has highest average velocity of ~500 m yr^{-1} (Figure 2, 3). The next ~6 km above from ice fall to the upper reaches of the accumulation zone comprise the third zone (Z3) where the average velocity is ~40 m yr^{-1}.

Surface velocities for the main trunk of Hispar glacier are at their highest near the ice fall (Figure 2). The tributary glaciers move at similar velocities to that of the trunk glacier. The velocity estimates revealed that the mean velocity of the main glacier trunk increased from 275 m yr^{-1} during 2013-14 to 344 m yr^{-1} during 2014-15. The mean velocity increased slightly by 10 m yr^{-1} reaching a maximum of 355 m yr^{-1} in 2015-16 before significant decelerating to 222 m yr^{-1} during 2016-17 period. The analysis of the velocity estimates and the visual inspection of the satellite data suggest that the surge started to build by 2013-2014 with the velocity increasing to 910 m yr^{-1}, the highest in the entire observation period of 5 years from 2013-2017 (Figure 2a). The surge wave, however, remained restricted to the accumulation zone on Hipsar Glacier, above the confluence with T4 (Figure 3). Relatively low velocities are seen below the confluence with T4 to the snout (Figure 2a, 3). Velocities on the Hispar Glacier are similar during the next observation period (2014-15) to those in the period 2013-14, although the surge wave advanced to the confluence with T1. Below this point there are negligible changes in the velocity between the two observation periods (Figure 2b). Although a small decrease in the maximum velocity from 910 m yr^{-1} in 2013-2014 to 863 m yr^{-1} in 2014-2015 was observed, the average velocity remained similar. The average velocity of the Hispar Glacier slightly increased in the year 2015-2016 compared to the previous periods of 2013-2014 and 2014-15 (Figure 2c). The surge front still persisted and protruded to its maximum up to the confluence with tributary T1 during the 2015-16 assessment period before sharply retreating back during 2016-17 period (Figure 2d). The surge front emerging near T4 at an altitude of ~3970 m amsl in 2013 moved down the glacier by ~10 km reaching the confluence point of T1 with the main glacier in 2016. The velocity pattern of the tributaries for the year 2015-2016 did not change much compared to

the previous assessment periods. Although no significant change in the velocity of the glacier snout was observed, inspection of the optical satellite data revealed that the glacier had expanded laterally. The analysis of the velocity maps of the Hispar Glacier suggest that that active phase of the surge started in the year 2013-2014, probably initiated by the acceleration of the T4 and T5 tributaries. The deformation of the medial moraine of the glacier trunk, a common characteristic of the surging tributaries at the confluence of these tributaries, also suggests their influence on the flow instability of glacier trunk (Paul et al., 2017). The Hispar Glacier trunk started to move at the similar velocity to that of its tributaries from 2013-14 to 2015-15 period. Our analysis suggests that the surface velocity of the glacier drastically decreases below point A (Figure 3) to the terminus and that the surge front never extended beyond T1, indicated by very low velocities of less than 1 m yr^{-1} in this zone. The velocity of the contributing tributaries (T4 and T5, Figure 2, 3) that converge with the main trunk below the icefall are considerably higher resulting in the initiation of the accelerated flow of glacier trunk. The mean velocity of the main glacier trunk during 2013-2014 was 280 m yr^{-1} while the tributaries T4 and T5 moved at 445 m yr^{-1} and 340 m yr^{-1} respectively.

In addition, Figure 2 indicates that the ice dynamics of the main glacier trunk is largely governed by the northern tributaries (T4 and T5). The influence of the northern tributaries is delimited by deformation of medial moraines originating from the main glacier trunk. Out of the five northern tributaries, the influence of the T4 and T5 is indicated by the development of a bulge and migration of the central moraine running along the main glacier trunk (Figure 2, 3). The bulge and migration of the central flow line again at the convergence of the T1 tributary with the main glacier trunk suggest comparatively higher velocity and ice flux of the tributary (Figure 3). It

is in this region most of the supraglacial ponds are formed as the surge front has never reached as far as this region in recent years (Gardelle et al., 2013; Paul et al., 2017). The surge of Hispar glacier did not propagate beyond T1 that could be explained by escape of water through the glacier bed as suggested by Smith et al. (2002), resulting in the drop of the basal water pressure and consequent halt in glacier surge.

3.2. Changes in glacial surface features

We analysed the optical satellite data from 2013 to 2017 for glacier surface changes. Distinct changes were observed in the supraglacial features from 2013 to 2015 (Figure 4). Very few surface features and the associated changes are recognisable on the satellite images of 2016 and 2017 which could be attributed to the cessation of the surge in that period. As such we provide here the detailed discussion on the glacier surface dynamics between 2013 and 2015.

Our analysis indicated that between September 2013 and September 2015 the glacier surface debris became concentrated in the lower ablation zone of the glacier. The formation and variations in the distinct features of looped and folded medial moraines also suggest the active surge phase of the glacier. On the glacier as whole, the area of debris cover reduced from ~118 km^2 to ~95 km^2, equivalent to a ~ 19% decrease from 2013 to 2017 (Figure 4). We note that the 2015 image has more snow cover than the others so we supplemented the debris delineation using high resolution Google Earth data. The reduction or complete disappearance of debris cover could be attributed to opening of numerous crevasses thereby transporting the debris into an englacial system (Bolch et al. 2017), a typical surge related phenomena. Distinct features, including looped and folded medial moraines, a characteristic feature of surge type glaciers (Meier and Post., 1969, Grant et al.,

2009), were also observed and mapped from the satellite imagery of 2015 (Figure 4). Such features were very sparse or at least not identifiable on satellite imagery of 2013, providing further evidence that the glacier entered its surge phase between September 2013 and September 2015. The influence of the northern tributaries on the glacier dynamics is more pronounced than the tributaries on the southern side, indicated by migration of the central moraine running along the main glacier trunk (Figure 4). The shift and bulging of the central moraine is more prominent near the confluence of T4 with the main glacier where migration of 80 m in the central moraine is observed.

The lateral expansion of the glacier tongue and the forward movement of surface features is also very prominent on the satellite images. Even though, the contributing tributaries do not show any significant change in their width, however a significant change in the width of the main glacier trunk was observed between 2013 and 2017. The expansion of the main glacier trunk was more evident below T4. Lateral expansion by 140 m from 2013 to 2017 was observed between T2 and T3. The lateral expansion continued as the glacier moved further downwards. An expansion of 240 m in the lateral extents of the glacier was observed near the confluence of T1 with the main glacier. The lateral expansion was limited to T1 as the surge front does not reach beyond this point. A mass wave related to the glacier surge front travelling down the glacier is clearly revealed from the satellite images between 2013 and 2015. The reduction and disappearance of the glacier ponds is also visible on the satellite images.

3.3. Changes in supraglacial water bodies

The supraglacial water bodies on the glacier were mapped as ponds and lakes; 183 supraglacial water bodies were identified on the glacier surface on the

September 2013 satellite image, out of which 165 (with area< 0.5 ha) were classified as ponds and the remaining 18 (with area > 0.5 ha) as lakes. The analysis of supraglacial water bodies revealed that they have reduced considerably both in number and size from 2013 to 2017 (Table 2, Figure 5). The number of supraglacial water bodies reduced from 183 in 2013 to 48 in 2017, corresponding to an area change of 121.63 Ha. The number of supraglacial lakes reduced from 18 to 4 while the number of supraglacial ponds reduced from 165 to 44 during the analysis period. This corresponds to an area change of 9.40 Ha and 22.0 Ha for lakes and ponds respectively. The disappearance and reduction of supraglacial water bodies from 2013 to 2017 again suggests accelerated velocity and ice flux, a characteristic of active surges, in 2017 compared to that of 2013. Glacier fracturing during the surge allows the accumulated water to either enter into englacial hydrological system or escape through the glacier bed. As a result, reduction or complete disappearance of many water bodies was observed post surge.

4. Conclusions

We have identified a surge of Hispar Glacier in the Karakoram between September 2013 and 2015. During the surge, velocities in the main trunk of Hispar Glacier reached a maximum of ~900 m yr^{-1}. The analysis of velocity together with the characteristic surge-type glacier features such as folded and contorted debris structures also indicate that the Hispar Glacier was in its active surge phase between September 2013 and September 2015. The rapid velocities were accompanied not only by changes in the surface debris distribution but also by a reduction in the number and size of supraglacial lakes and ponds between 2013 and 2015. It was further demonstrated that the flow instability on the main trunk of Hispar glacier is determined by the dynamics of the tributary glaciers.

Acknowledgements

The authors express gratitude to the three anonymous reviewers for their valuable comments and suggestions on the earlier versions of the manuscript that have greatly improved the content and structure of the manuscript.

References

Barrand NE, Murray T. 2006. Multivariate controls on the incidence of glacier surging in the Karakoram Himalaya. Arctic, Antarctic, and Alpine Research 38(4) : 489-498. DOI: 10.1657/1523-0430(2006)38[489:MCOTIO]2.0.CO;2

Bolch T, Pieczonka T, Mukherjee K, and Shea J. 2017. Brief communication: Glaciers in the Hunza catchment (Karakoram) have been nearly in balance since the 1970s. The Cryosphere, 11, 531-539. DOI: 10.5194/tc-11-531-2017

Copland L, Sylvestre T, Bishop MP, Shroder JF, Seong YB, Owen LA, Bush A, Kamp U. 2011. Expanded and recently increased glacier surging in the Karakoram. Arctic, Antarctic, and Alpine Research 43(4) : 503-516. DOI: 10.1657/1938-4246-43.4.503

Gardelle, J., Berthier, E., Arnaud, Y., & Kaab, A. (2013). Region-wide glacier mass balances over the Pamir-Karakoram-Himalaya during 1999-2011 .Cryosphere, 7(6), 1885-1886. DOI: 10.5194/tc-7-1885-2013

Gardner JS., Hewitt K. 1990. A surge of Bualtar Glacier, Karakoram Range, Pakistan: a possible landslide trigger. Journal of Glaciology 36(123): 159-162. DOI: 10.3198/1990JoG36-123-159-162

Grant KL, Stokes CR, Evans IS. 2009. Identification and characteristics of surge-type glaciers on Novaya Zemlya, Russian Arctic. Journal of Glaciology 55(194) : 960-972. DOI: 10.3189/002214309790794940

Heid T, Kääb A. 2012. Evaluation of existing image matching methods for deriving glacier surface displacements globally from optical satellite imagery. Remote Sensing of Environment 118 : 339-355. DOI: 10.1016/j.rse.2011.11.024

Herreid S, Pellicciotti F, Ayala A, and Chesnokova A. 2015. Satellite observations show no net change in the percentage of supraglacial debris-covered area in northern Pakistan from 1977 to 2014. Journal of Glaciology, 61, 524-536. DOI:10.3189/2015JoG14J227, 2015.

Hewitt K. 1969. Glacier surges in the Karakoram Himalaya (Central Asia). Canadian Journal of Earth Sciences 6(4) : 1009-1018. DOI: 10.1139/e69-106

Hewitt K. 1998. Glaciers receive a surge of attention in the Karakoram Himalaya. Eos, Transactions American Geophysical Union 79(8) : 104-105. DOI: 10.1029/98EO00071

Hewitt K. 2005. The Karakoram anomaly? Glacier expansion and the 'elevation effect,' Karakoram Himalaya. Mountain Research and Development 25(4) : 332-340. DOI: 10.1659/0276-4741(2005)025[0332:TKAGEA]2.0.CO;2

Hewitt K. 2007. Tributary glacier surges: an exceptional concentration at Panmah Glacier, Karakoram Himalaya. Journal of Glaciology 53(181) : 181-188. DOI: 10.3189/172756507782202829

Kääb A, Volmer M. 2000. Surface geometry, thickness changes and flow fields on creeping mountain permafrost: automatic ex-traction by digital image analysis. Permafrost and Periglacial Processes 11 : 315-326. DOI: 10.1002/1099-1530(200012)11:4<315::AID-PPP365>3.0.CO;2-J

Kääb A. 2005. Remote sensing of mountain glaciers and permafrost creep. Geograph. Inst. d. Univ.; 2005. Available at: http://folk.uio.no/kaeaeb/publications/habil_screen.pdf

Mayer C, Fowler AC, Lambrecht A, Scharrer K. 2011. A surge of North Gasherbrum Glacier, Karakoram, China. Journal of Glaciology 57(205) : 904-916. DOI: 10.3189/002214311798043834

Meier MF, Post A. 1969. What are glacier surges? Canadian Journal of Earth Sciences 6(4) : 807-817. DOI: 10.1139/e69-081

Paul, F., Strozzi, T., Schellenberger, T., & Kääb, A. (2017). The 2015 Surge of Hispar Glacier in the Karakoram. Remote Sensing, 9(9), 888. DOI: 10.3390/rs9090888

Quincey DJ, Braun M, Glasser NF, Bishop MP, Hewitt K, Luckman A. 2011. Karakoram glacier surge dynamics. Geophysical Research Letters 38 (18). DOI: 10.1029/2011GL049004

Quincey DJ, Glasser NF, Cook SJ, Luckman A. 2015. Heterogeneity in Karakoram glacier surges. Journal of Geophysical Research: Earth Surface 120(7) : 1288-1300. DOI: 10.1002/2015JF003515

Rashid I, Abdullah T. 2016. Investigation of temporal change in glacial extent of Chitral watershed using Landsat data: a critique. Environmental Monitoring and Assessment 188(10) : 546. DOI: 10.1007/s10661-016-5565-z

Rashid I, Romshoo SA, Muslim M and Malik AH. (2010). Landscape level vegetation characterization of Lidder valley using geoinformatics. Journal of Himalayan Ecology and Sustainable Development, 6, 11-24.

Sevestre H, Benn DI. 2015. Climatic and geometric controls on the global distribution of surge-type glaciers: implications for a unifying model of surging. Journal of Glaciology 61(228) : 646-662. DOI: 10.3189/2015JoG14J136

Smith AM, Murray T, Davison BM, Clough AF, Woodward J, and Jiskoot H. 2002. Late surge glacial conditions on Bakaninbreen, Svalbard, and implications for

surge termination. Journal of Geophysical Research: Solid Earth, 107(B8). DOI: 10.1029/2001JB000475

Vollmer M. 1999.Kriechenderalpiner Permafrost: Digitale photo-grammetrische Bewegungsmessung. Doctoral dissertation, Diploma thesis, Department of Geography, University of Zurich.

Workman FB. 1908. Further Exploration in the Hunza-Nagar and the Hispar Glacier. The Geographical Journal 32(5) : 495-496. DOI: 10.2307/1777169

Workman FB. 2010. The Hispar Glacier: Its mountains and tributaries. The Geographical Journal 35(2) : 105-115. DOI: 10.2307/1776943

Figure Captions:

Figure 1: Location of Hispar Glacier in the Karakoram. Background elevation data is from ASTER GDEM v2.

Figure 2: Annual velocity estimates (m yr^{-1}) of Hispar glacier based on Landsat 8 OLI satellite data for (a) 2013-14 (b) 2014-15, (c) 2015-16 and (d) 2016-17.

Figure 3: The Hispar glacier after the surge. The surge front is indicated by the red arrow and the glacier terminus is indicated by the blue arrow. Letters indicate different velocity zones explained in the text and the tributaries (T1 to T5) of the glacier.

Figure 4: Glacial geomorphological features of Hispar Glacier mapped from Landsat 8 OLI from 2013-2017. The panels on the left (a-e) are Landsat False Colour Composite (FCC) image of Landsat 8 OLI and the panels with an asterisk (*) on the right (a*-e*) depict the glacial geomorphic features for the corresponding year. (a) 2013, (b) 2014, (c) 2015, (d) 2016 and (e) 2017

Figure 5: Mapping of supraglacial water bodies from Landsat 8 OLI satellite images (a) 2013, (b) 2014, (c) 2015, (d) 2016, and (e) 2017

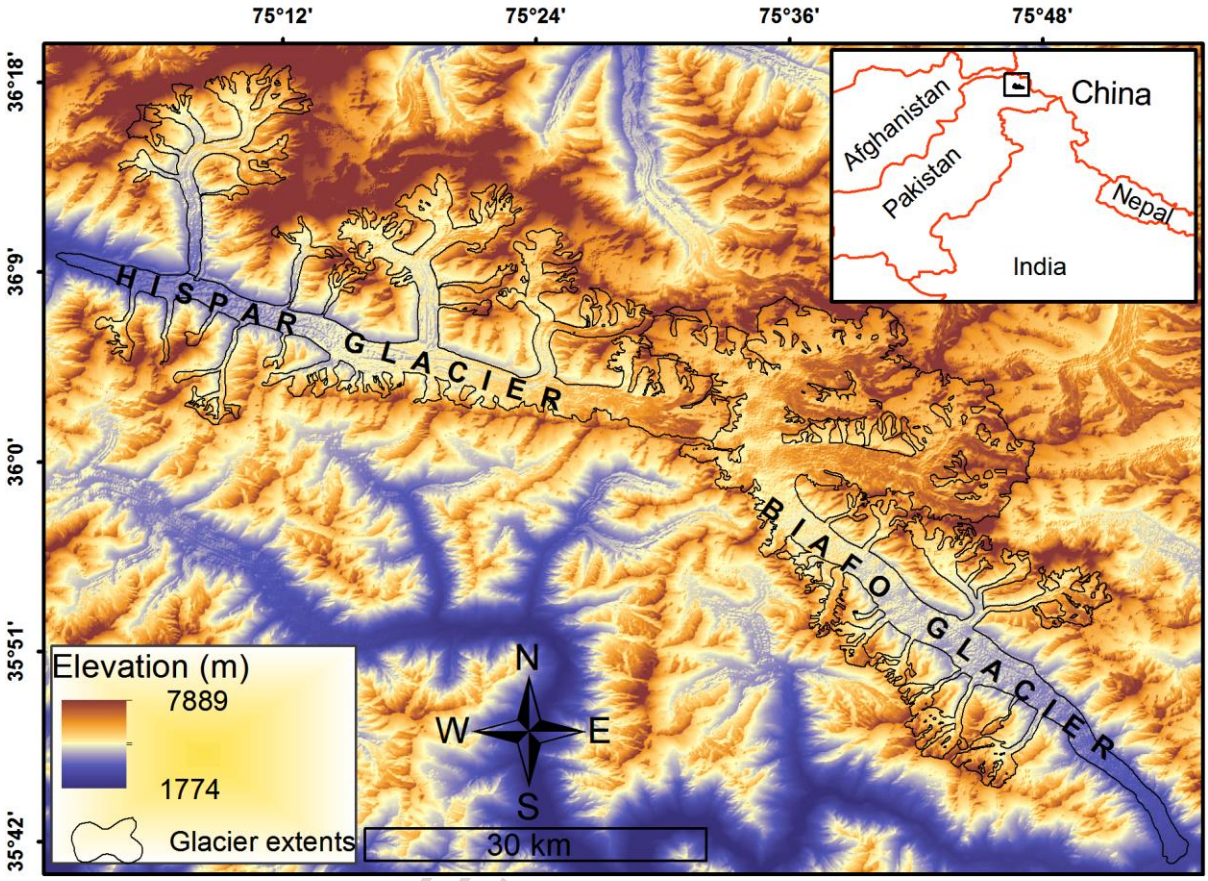

Fig. 1

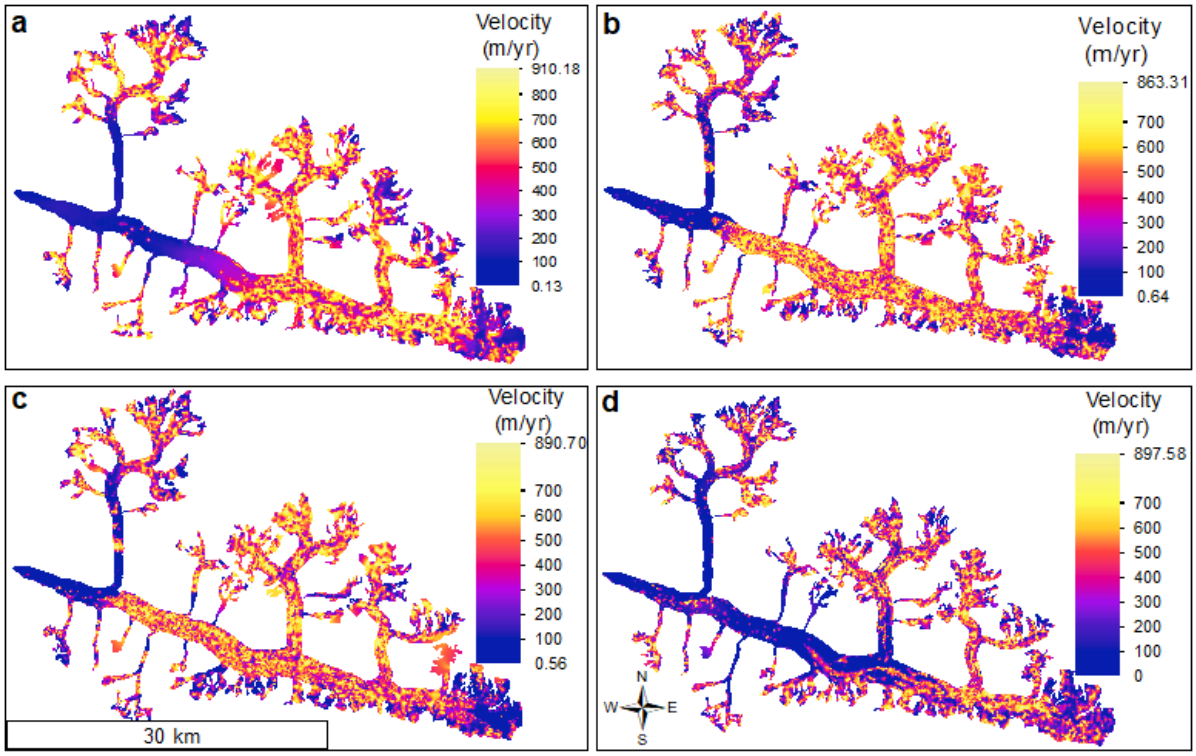

Fig. 2

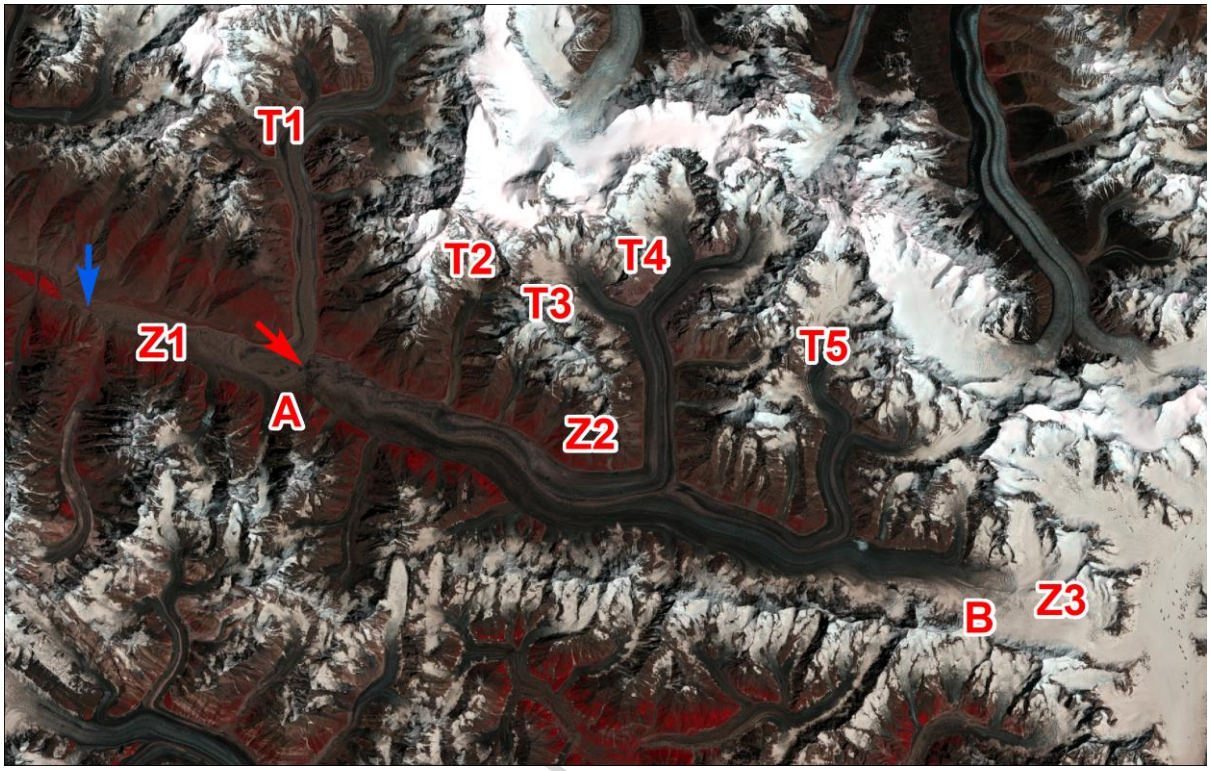

Fig. 3

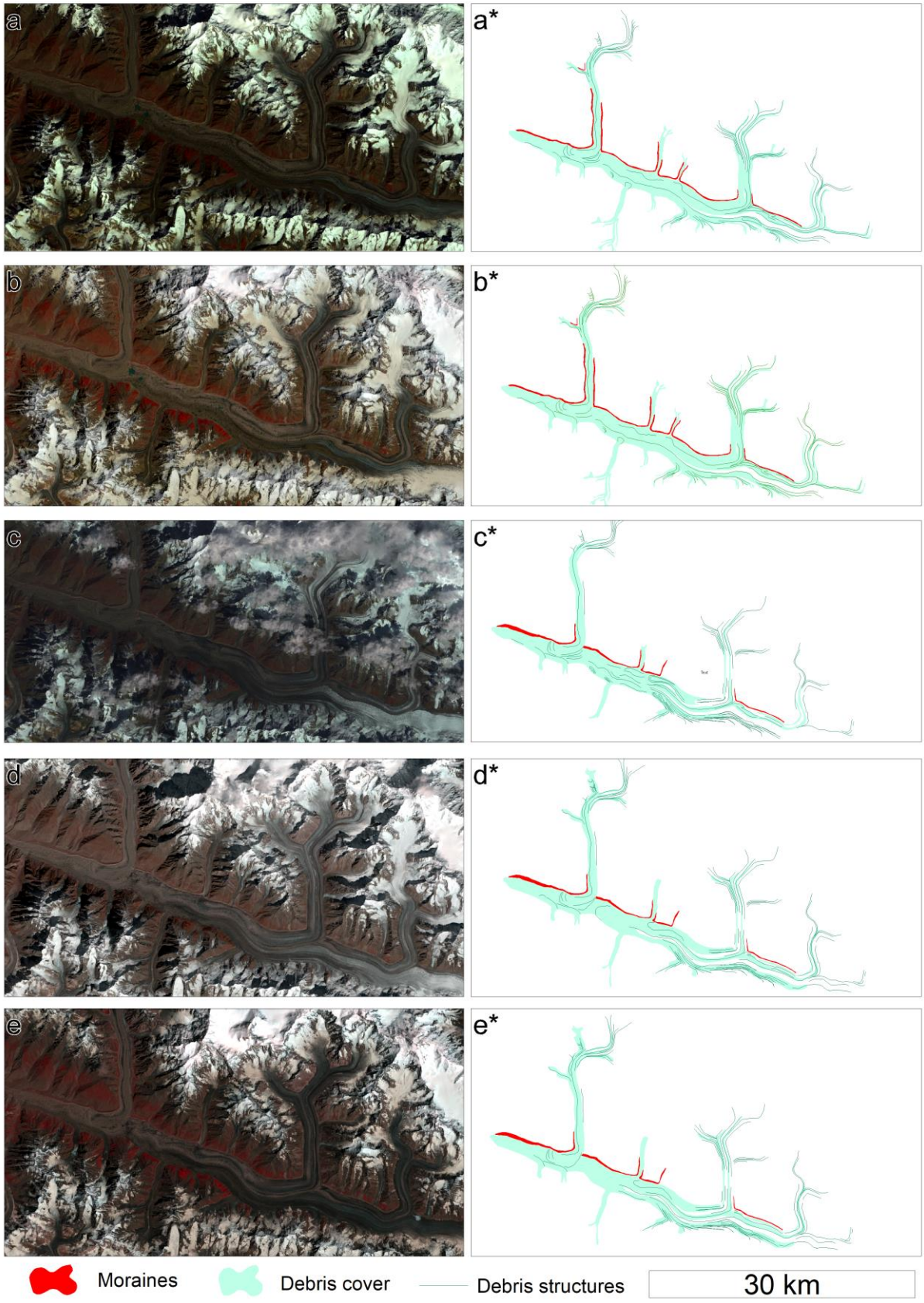

Fig. 4

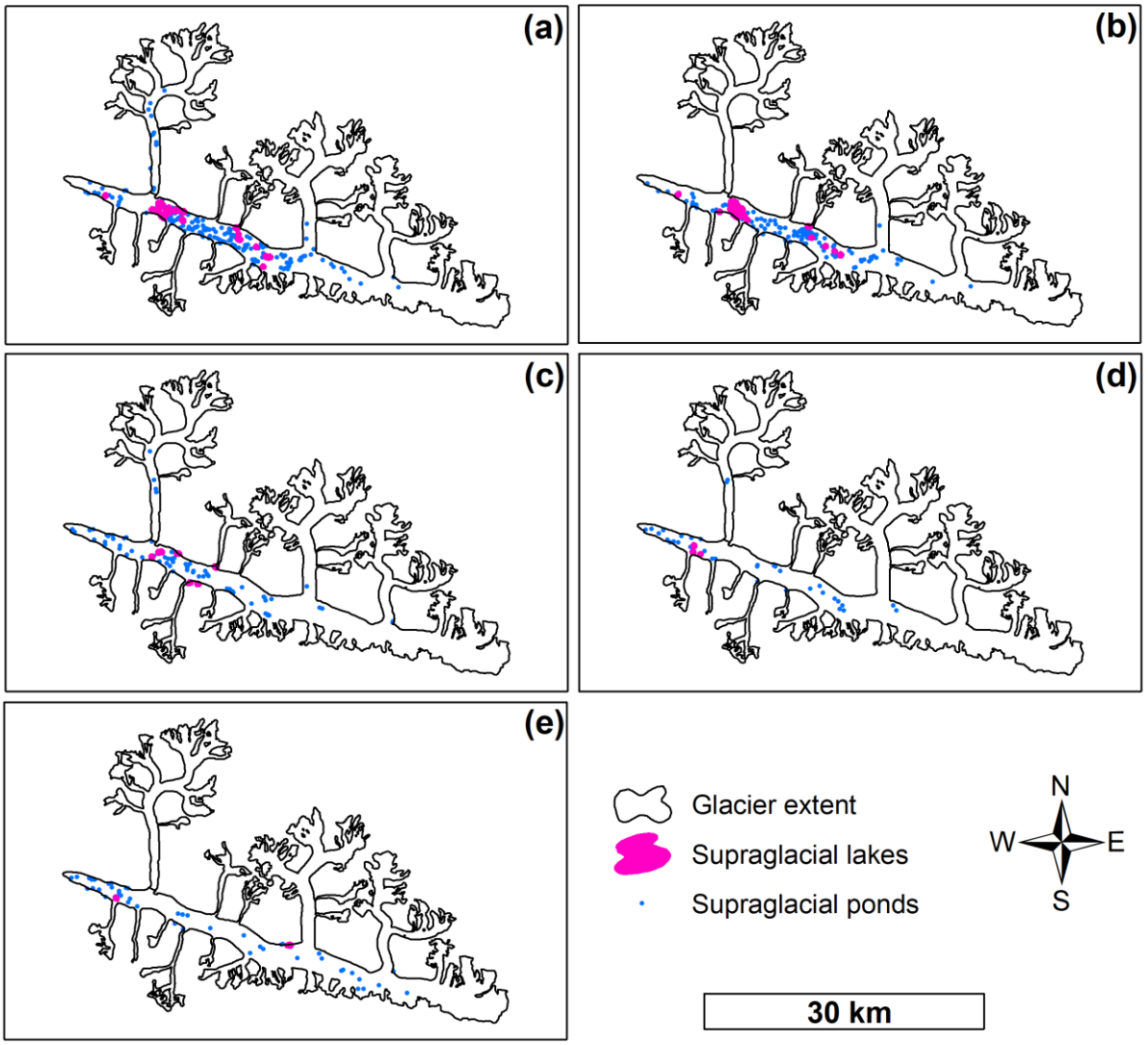

Fig. 5

Table 1: Characteristics of datasets used in the study

Scene ID	Sensor	Date
LC81490352013250LGN00	Landsat 8 OLI	09 September, 2013
LC81490352014253LGN01	Landsat 8 OLI	10 September, 2014
LC81490352015256LGN00	Landsat 8 OLI	13 September, 2015
LC81490352016275LGN01	Landsat 8 OLI	01 October, 2016
LC81490352017213LGN00	Landsat 8 OLI	01 August, 2017

Table 2: Changes in supraglacial water bodies on Hispar Glacier between 2013 and 2017. Numbers in brackets indicate area of ponds and lakes in Hectares

	2013	**2014**	**2015**	**2016**	**2017**	**Change (2013-2017)**
Ponds	165 (66)	103(51.5)	67 (26.8)	41(20.5)	44(22)	121(40)
Lakes	18 (87.03)	16 (70.30)	6 (17.71)	5(5.14)	4(9.40)	14 (77.63)
Total	183 (153.03)	119(121.8)	73 (44.51)	46 (25.64)	48(31.4)	135 (121.63)

Highlights:

- Remote sensing methods were used to assess changes in the velocity of Hispar Glacier between 2013 and 2017
- A glacier surge impacted the distribution of supraglacial debris and medial moraines
- Changes in supraglacial water bodies were estimated from 2013-2017
- Flow instability is controlled by the dynamics of the tributary glaciers of Hispar Glacier